ATTENUATION OF LAMB WAVES USING EMBEDDED SEISMIC METAMATERIALS FOR LOW-FREQUENCY BANDGAP

Collins OPASINA [1], Akintoye OYELADE [2, *] Yetunde O. ABIODUN [3], OLUWASOLA O. ORIBAYO [4]

This study investigates the performance of Seismic metamaterials (SM) embedded in a soil substrate, exploring four SM models incorporating materials such as lead, auxetic foam, and soil in the outer layer. Four types of SM models containing lead, auxetic foam and soil at the outer layer are proposed in the study. The finite element method was adopted to investigate the dispersion curves of Lamb waves and vibration modes of these periodic structures. The relationship between structural parameters, geometric sizes and bandgap characteristics were analyzed. Model 3 turned out with the widest favorable result of 2.4-6.8Hz which is within the low frequency range of concern.

Keywords: seismic metamaterial, bandgaps, lamb waves, low frequency bandgap.

1. Introduction

As the need for urbanization increases daily, so is the need for the rising demands of civil infrastructures. Beyond just satisfying the housing and immediate needs which is the primary goal of most infrastructural development, the need to look deeply into sustainability and risk mitigation in the occurrence of natural disaster is also of paramount importance. Seismic events associated with earthquakes ranks top in naturally occurring catastrophic activities that severely destroys lives and human settlement. Hundreds of earthquakes occur globally every year, with over a thousand having magnitudes of 5 or higher. In the event of an earthquake, the seismic waves generated carry intense energy outward from it center to all directions. Earthquakes frequency wave between 0–20 Hz coincides with the resonant frequencies of most civil infrastructures [1]. Conventional seismic control methods like base isolation, and energy dissipation often struggle to

* Corresponding author
[1] Mr., Department of Civil and Environmental Engineering, Faculty of Engineering, University of Lagos, 100213, Nigeria, e-mail: Collinsopasina66@gmail.com
[2] Dr., Department of Civil and Environmental Engineering, Faculty of Engineering, University of Lagos, 100213, Nigeria, e-mail: aoyelade@unilag.edu.ng
* Corresponding author
[3] Dr.., Department of Civil and Environmental Engineering, Faculty of Engineering, University of Lagos, 100213, Nigeria, e-mail: yabiodun@unilag.edu.ng
[4] Dr., Department of Chemical Engineering, Faculty of Engineering, University of Lagos, 100213, Nigeria, e-mail: ooribayo@unilag.edu.ng

effectively control or isolate ultra-low-frequency seismic waves within 0–20 Hz. This drawback has led researchers to take a closer look into phononic crystals and metamaterial for ability to manipulate acoustic waves. Towards the end of the 20th century, phononic crystals was introduced with the ideology of them having the ability to control elastic waves in geometric structure. They possess periodic acoustic effects which allows the prevention of elastic wave propagation. Phononic crystals and metamaterials share a relationship of artificial structures that are able to manipulate photon propagation [2] . Bandgap BG formation in phononic crystal was due to local resonance that contributed to shock and noise reduction [3]. Figure 1 shows the various forms in which phononic crystals can exist.

Seismic metamaterials (SM) effectively attenuate seismic waves without altering the building's structural form [4]. SM are designed artificially with periodic arrangements that enables BG characteristics [5]. Waves falling in b regions are restricted to pass through SM, which are situated in specific position of interest around the buildings to dampen seismic waves [6]. Various classification methods exist for SM based on different perspectives [7-9]. Bragg scattering and local resonance exists as the major bandgap formation mechanism [10]. In Bragg scattering, SM structures size is proportional to wavelengths where structural periodicity determines the properties outcome [11-13]. However, the wavelength of seismic waves can vary from few to several meters, limiting the application range of such SM. On the other hand, local resonant SM have structural dimensions 2–3 orders of magnitude smaller than seismic waves with the limitation of smaller bandgaps [14]. In fighting these limitations, scholars have suggested different structural variations, including the "rainbow trap"[15, 16], additive structures [4, 17], structural steel of I section [18] and composite steel material [7] in half-space also improve the attenuation of Rayleigh waves. An uncommon material like depleted uranium [19], auxetic foam instead of common steel or rubber inclusion in structural composition has been used to improve the bandwidth [16]. Natural occurring SM effects are discovered in arrays of forest trees [20]. In expounding on forest trees as SM, the impact of tree branches in Rayleigh waves attenuation was investigated to yield a considerable effect [21]. The relationship of layer properties in the isolation and shielding of seismic activities was also studied for soils with non-homogeneity across its strata [22].

Taking a close look into the post build challenges facing civil infrastructures, studies have shown that more than ten thousand structures made of load bearing frames of concrete and steel are vulnerable to seismic activities due to large energy and vibrations. In combating this compromise, the inclusion of metamaterials in foundation construction became an area of interest. Metamaterials have the ability to manipulate vibrations in structural components [23, 24]. Metamaterial also produced a shielding effect when included in foundations of buildings in earthquake occurrence [25]. The overlaying superstructure are

protected as the propagation of seismic wave was prevented due to the presence of periodic materials in the structural foundation [26]. Wave manipulation effect in solids is attributed to transmission of energy in a wave manner and the effectiveness of periodic materials in stopping waves from propagation. In investigating periodic structures with three-dimensional geometry, attenuation is possible only within the bandgap formation zones and the wave amplitude have a reduced effect within this region [27, 28].

Four types of SM was identified in recent time according to [29], seismic soil metamaterials [6], auxetic materials [30], above-surface resonators [31], and buried mass resonators [14]. In SM study, options including structural steel types [13], unit cell geometry [32], and steel sections buried within soil mass [33].The application of SM goes beyond building protection and branches to insulation of railway systems. Currently, the practical implementation of existing geometric forms of Lamb wave attenuation designs are difficult to achieve because of the large size associated with them. Greater challenges are faced in achieving bandgaps of low frequency with SM having small geometric configuration.

The study focused on finite element analysis of periodic structures with the aim to design a seismic metamaterial that inhibits low frequency (0 - 20Hz) wave propagation within adjoining structure. To proffer solution to the established challenges, four models were designed to address the constraint of large structural form and low frequency gaps. The objectives of the study include investigating geometric model suitable for the desired bandgap, studying the wave propagation and interaction within the constituent seismic metamaterial and to verify the attenuation zone within the seismic metamaterial using transmission spectrum. To achieve all these, the study was divided into four sections, where Section 1 introduces the concept and gave a background of the study through review of literatures. In Section 2, the theory behind the study was explained alongside the methodology. The discussion of the result was explained in Section 3, while the conclusion of the findings and further recommendations was made in Section 4.

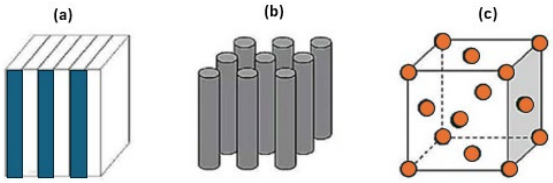

Fig. 1. Representation of phononic crystals: (a) 1-dimensional (b) 2-dimensional (c) three dimensional

2. Theory and methodology

2.1. *Periodic wave equation*

Assuming a perfectly elastic homogeneous and isotropic medium, the wave motion equation propagating through the periodic system when damping and body force is neglected is expressed as [34]

$$\Delta\big(C(r):\Delta u(r)\big) = -\rho(r)\omega^2 u(r), \tag{1}$$

where Δ is the Hamiltonian operator, the location vector denoted by $\boldsymbol{r}$, the displacement vector as $\boldsymbol{u}$, $\boldsymbol{\omega}$ as angular frequency, $\boldsymbol{C}$ is the fourth-order elasticity tensor, ρ is the mass density of constituent material. The unit cell under the Floquet-Bloch parametric end conditions was studied to investigate the propagating waves in periodic structures as shown in Fig 2.

The boundary behavior with respect to periodicity is given by [35]

$$u(r+a) = u(r)e^{ika}, \tag{2}$$

where $\boldsymbol{a}$ is the lattice vector, and $\boldsymbol{k} = [k_x \quad k_y]$ the wave vector, and $i = \sqrt{-1}$. Substituting (2) in (1) results

$$(K(k) - \omega^2 M)u = 0, \tag{3}$$

where k and M are the stiffness matrix and the mass matrix, respectively, which are functions of the wave vector $\boldsymbol{k}$. COMSOL Multiphysics 5.6 is used to solve the eigenvalue problem given by (3) under the complex boundary condition. For a given wave vector $\boldsymbol{k}$, there exists frequency $\boldsymbol{\omega}$ that can obtain the dispersion relation. Sweeping the frequency along the edges of the first irreducible Brillouin zone along $\Gamma - X - M - \Gamma$, the total dispersion relations are obtained. The representative unit cell of the corresponding Brillouin zone is shown in Fig. 2.

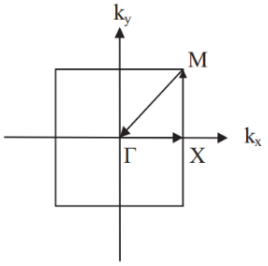

Fig. 2. Schematic representation of the first irreducible Brillouin zone for a square lattice arrangement

2.2. *Comparison and verification*

Verification of previous work was done in this section by comparing the dispersion curve results. The model was compared to the work done by previous researchers on Lamb waves [13, 36, 37], and there is a close agreement with the work as shown in Fig 3.

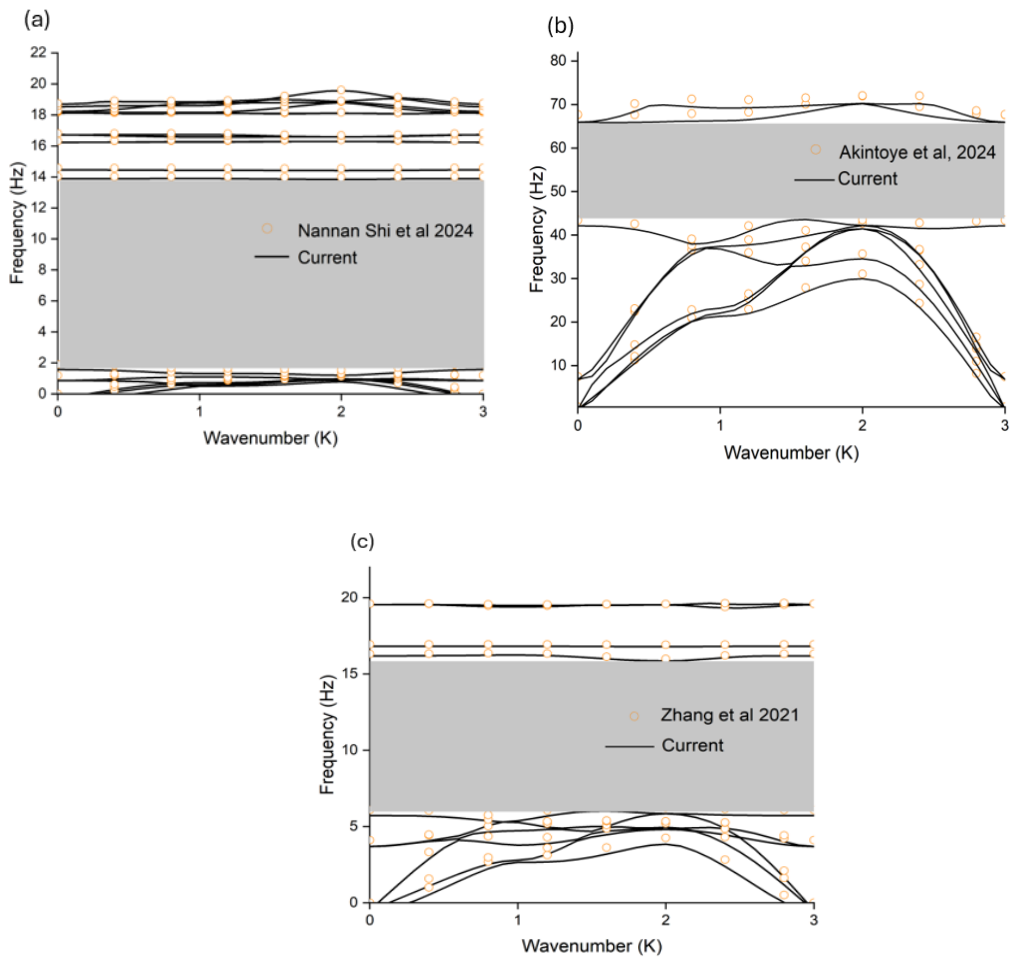

Fig. 3. Dispersion curve for Lamb wave from previous researchers (a) Nannan shi et al [36] (b) Akintoye et al [37] (c) Zhang et al [13]

2.3. *Models and methodology*

The designed model is made up of lead, auxetic foam, and soil as the outer layer. The design modified the models of [36]. In Fig 4 (a), the first model design has all material on the same level at the top, where the solid lead cube at the core of the design has side length of 1.4m is coated with auxetic foam with a face width of 2m, followed by the external coating of soil layer with a lattice constant a of 2.2m. In Fig 4(b), the design was modified with all materials boundaries having concentricity starting with solid lead of 1.58m on all sides at the center of the geometry, then a coating of auxetic foam around it with face width of 2m and lattice constant of 2.2m for the soil at the outer layer. The next is Fig 4(c), where the model improved on the structure in Fig 4(b) by having a lead core at the center with a cube side length of 1.6m, containing a cubic hole with a side length of 0.6m within it.

The last model as in Fig 4(d) has four circular perforations of 0.8m radius positioned on four side faces of the auxetic foam. Table 1 presents the parameters of the SM with their characteristic distinction. Fig 5. represents the plan view of the different configuration with the side view show in Fig 6.

Assuming periodicity in every direction, the wave vector is confined to the first Brillouin zone. The dispersion curve of the structure can be obtained by scanning the wave vector along the Γ-X-M-Γ direction of the first irreducible Brillouin zone. In verifying the accuracy of the BG and the attenuation characteristics for the finite-row (unit cell) structure, a 10x10 array design of the transmission spectrum was incorporated for the four models as shown Fig 7. Transmission spectrum calculation model was used in frequency-domain analysis for the model, with material properties given in Table 1. The perfect matching layer (PML) at outer bounds of the model is utilized to reduce the influence of elastic wave reflection on the results. Using the approach of Floquet periodic boundary conditions in the y direction, A displacement of 0.1 m was applied along the x-y polarization direction at the interface between the PML and the soil on the left side to simulate excitation of seismic waves in the Γ-X direction. The frequency scan vary from 0 to 20 Hz having 0.01 Hz increments. At the rear of the structure, the acceleration or displacement amplitude A1 is recorded. When there is no SM, the acceleration or displacement amplitude at the same point is recorded as A0, and the frequency response function FRF is defined as:

$$FRF = 20log10(A1/A0) \tag{4}$$

Table 1

Material Parameters of Seismic Metamaterial

	Density (kg/m3)	Elastic modulus (Pa)	Poisson's ratio
Soil	1200	12	0.3
Auxetic foam	120	2.5×10^4	-0.8
Lead	11340	1.7×10^{10}	0.42

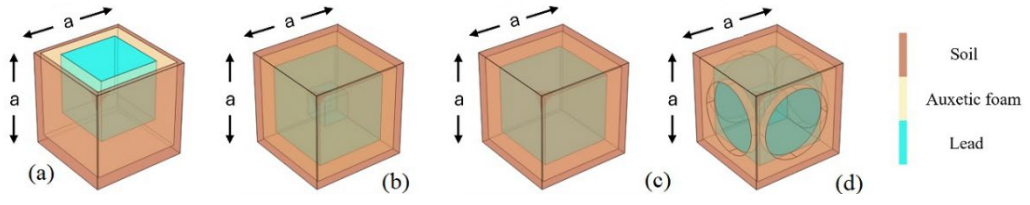

Fig. 4. Unit cell structure with lattice constant a =2.2m for (a) Model 1(b) Model 2 (c) Model 3 (d) Model 4

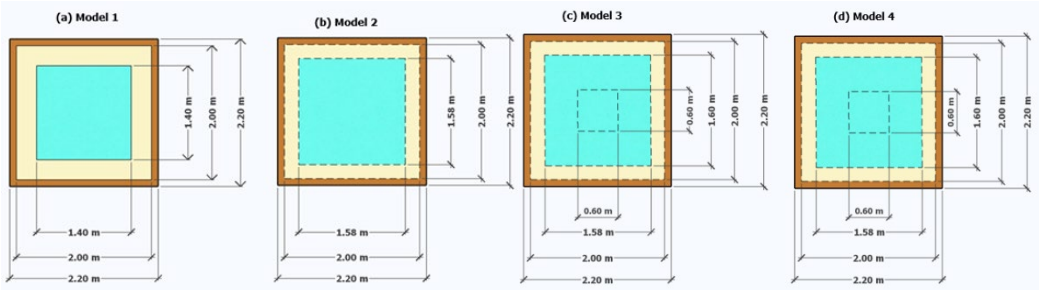

Fig. 5. Plan view of unit cell with geometric parameters

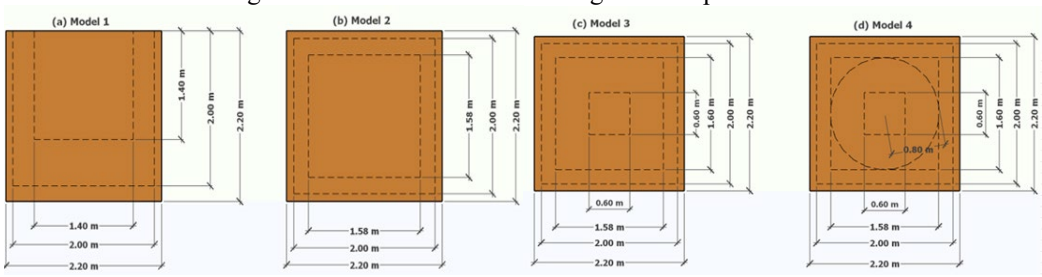

Fig. 6. Side view of the four models showing the internal details of the internal materials

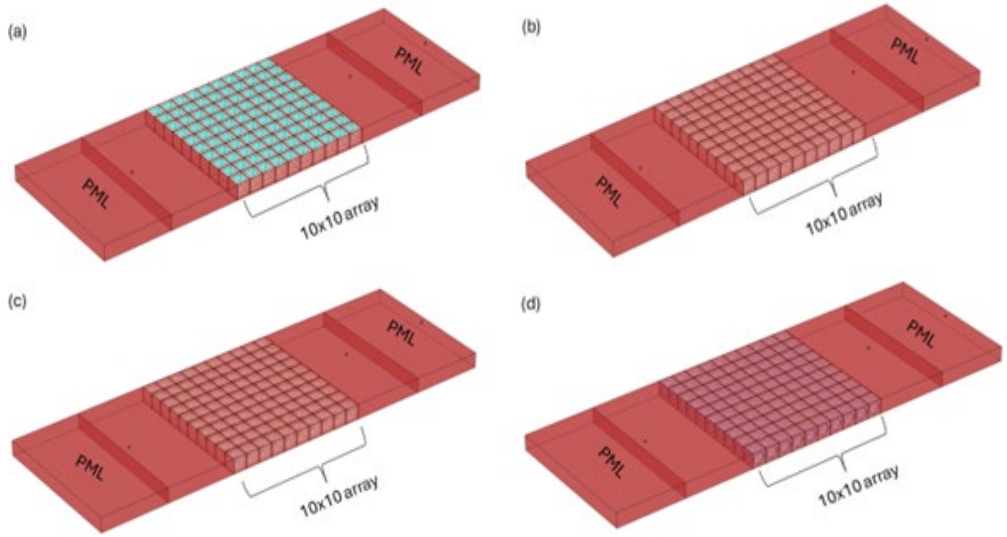

Fig. 7. 10x10 model setup representation of the infinite geometry for the four model types

3. Result and discussion

3.1. *Dispersion curve*.

Fig 8. displays the dispersion curves for the four structures, the first complete bandgap highlighted in brown shaded color with the upper and lower edges marked as red and blue shaded circles. Fig 8(a) gives the dispersion curve of Model 1, exhibiting a BG from 2.2Hz to 4.2Hz that exists between the fourth and

fifth frequencies. In Fig 8(b), the dispersion curve of Model 2 depicts a BG width from 2.4Hz to 6.6Hz in the sixth and seventh frequency bands, it is observed that the fully submerged soil coated design structure model possesses a larger relative bandwidth compared to Model 1 (with all top surface material on the same level). Fig 8(c) illustrates the dispersion curve of Model 3, with a BG width of 2.4 Hz to 6.8 Hz Based on this modification, it can be said that the geometric design of the fully concentric model having a cubic hollow opening of 0.6m exhibited a slight increase in bandgap compared to the model without an internal cubic opening as in model 2. Fig 8(d) represents the dispersion curve of Model 4, with a BG of 12.9 Hz to 13.9 Hz in the tenth and eleventh frequency bands. The design was achieved by opening circular holes in the four sides of the auxetic foam while still retaining the cubic hole in the lead core as in model 3. Compared to the rest of the models, it exhibited a higher frequency zone with a small bandwidth of 1Hz. In all, the models exhibited frequency range of great importance and application in isolation protection for building structures.

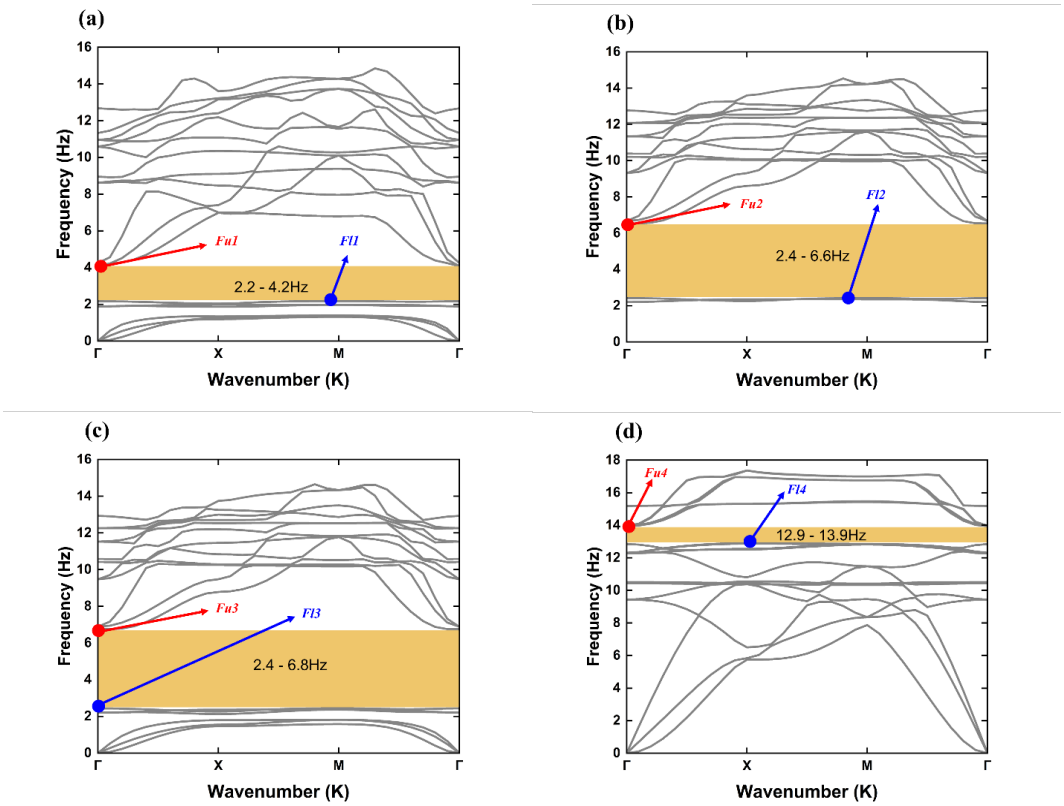

Fig. 8. Dispersion curve

3.2. *Vibration modes of unit cells*.

To further understand the concept of BG, the vibration behavior belonging to the two bounds of the first BG were studied. Fig 9. illustrates the vibration modes

of the upper and lower boundaries of four models. In Figure 11 (a), Fl1 represents the vibration mode of the lower boundary of Model 1 concentrated in the lead core (scatterer), leaving the auxetic foam and soil layer undisturbed. The Fu1 mode corresponds to the upper boundary of the bandgap of Model 1, with distinct vibration within the auxetic foam layer and soil layer. Fig 9(b) illustrates the vibration modes of the Fl2 and Fu2 of the respective lower and upper boundaries of the bandgap in Model 2. The lead core is completely buried in the entire matrix in all directions with no clear vibrations reaching to the surface as the case of Fl2. For Fu2, there is vibration radiating to outer surface of the soil with high concentration along the corners of the soil. The vibration modes of the lower and upper boundaries of the BG of Model 3 in Fig 9(c) are represented as Fl3 and Fu3. In the case of Fl3, the vibration stays within the lead core buried in the whole system and then gradually radiated faintly to the side face of the soil. The vibration was evidently displayed along the whole face of the soil, leaving the top face undisturbed at the center as in the case of Fu3. In Fig 9(d), the vibration modes for Model 4 as in Fl4 and Fu4 shows that the cubic hollow and circular cut in the lead and auxetic foam layer is responsible for the vibration mode behavior of Fl4 which is characterized by having vibrations in the top and bottom face corresponding to soil layer leaving the rest of the matrix undisturbed. In the case of Fu4, the mode resembles that of Fl4 with the vibration reaching further along the edge line of the soil layer leaving the auxetic foam undisturbed. Consequently, hole openings affect the BG and vibration behavior of the system.

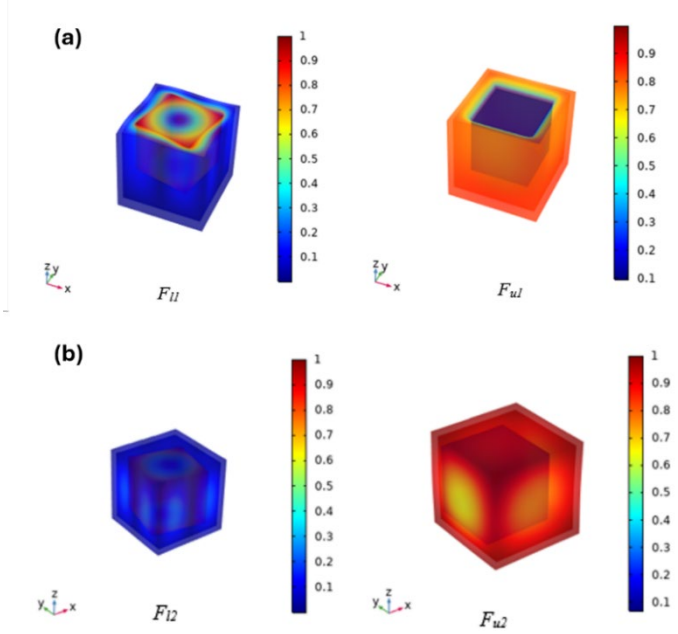

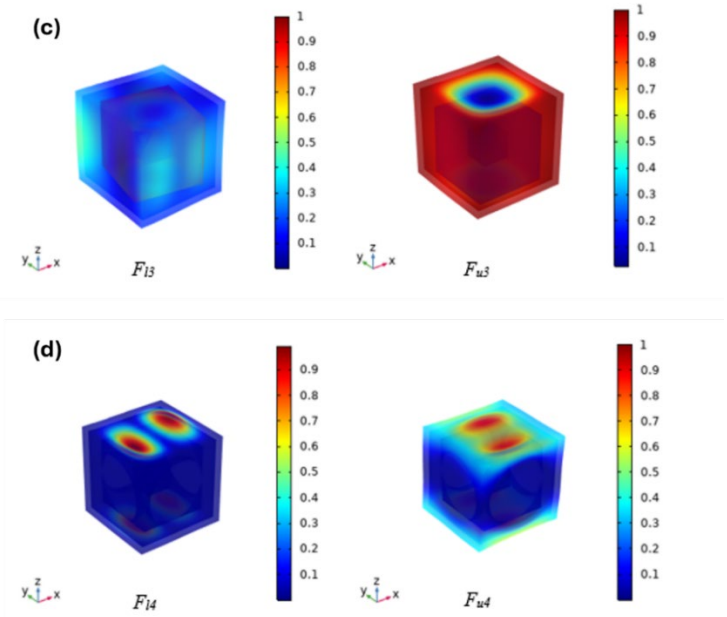

Fig. 9. Vibration mode shape for all models

3.3. Frequency-domain analysis.

Frequency spectrum analysis was used to better verify and gain insight into the ability of the proposed SM band gap formation mechanism. A homogenous soil layer was used in the implementation of the four different model type of the 10x10 unit cell surrounded by the soil. PMLs are placed after the soil. Then the transmission spectrum is obtained by sweeping from 0 Hz to 20 Hz along the x direction. According to Fig 10(a1-d1) corresponding to the transmission spectrum, the zones of elastic wave attenuation are observed in the following respective ranges 2.2–4.2 Hz, 2.4 –6.6 Hz, 2.4 –6.8 Hz, and 7.6–12.4 Hz, which is consistent with bandgap formation in Fig 8, except for the case of model 4. The dynamic response of the four models shown in Fig 12(a2-d2) clearly show that the soil embedded SM blocked propagation of wave in the bandgap region as vibration was not observed in the array of the SM.

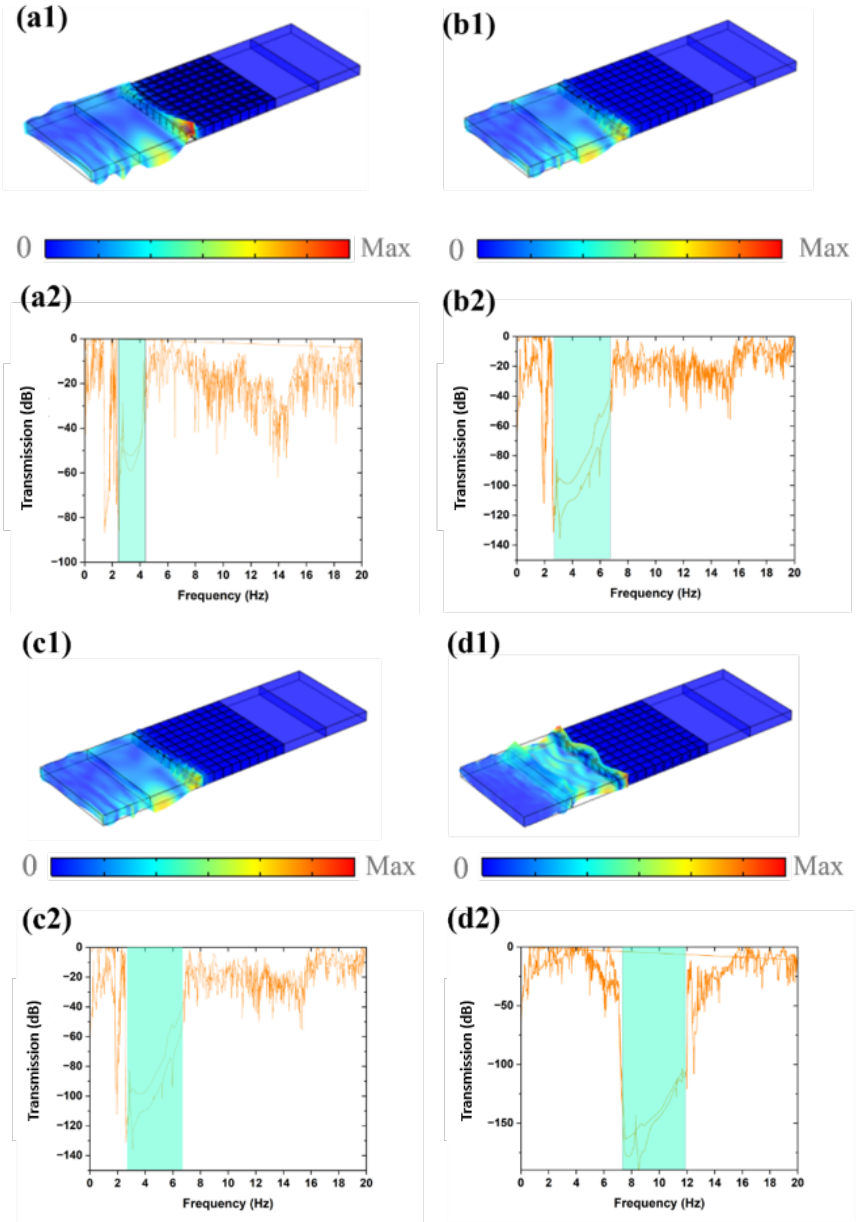

Fig. 10. Dynamic response and transmission spectrum for the four model shapes

3.4. Geometric parameter analysis.

The result from analysis in the preceding sections depicts that local resonance focused on the lead core causes low frequency curve BG in SM in the range of interest. Taking a closer look at the influencing factors corresponding to bandwidth with model 2 and 3 in mind, parameters of the models was examined by varying one parametric variable at a time while keeping all other constant. An

insight was presented to the behavior of these models as shown in the figures below. In Fig 11, the lattice constant was varied from 2.2m to 3m while all other parameters are kept constant. It was observed that the lower bandgap went on a gentle increase while the upper bandgaps decreased sharply. The total bandwidth reduces as the soil thickness increases within the SM. In Fig 12, the radius of the circular opening auxetic foam was varied from 0.2m to 0.8m while all other parameters are kept constant. It was observed that the lower bandgap increased sharply while the upper bandgaps saw a decrease along the line before increasing back. However, the total bandwidth reduced as the radius "r" increases.

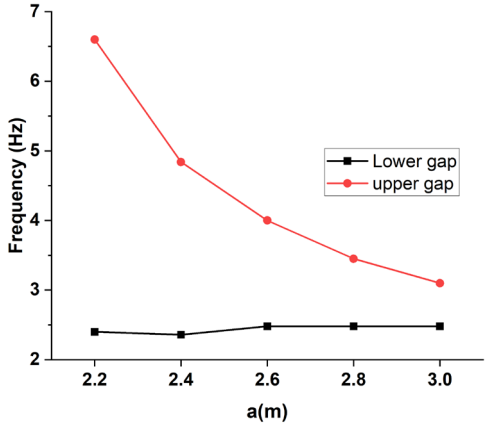

Fig. 11. Lower and upper bandgap variation with increase in lattice constant "a" for model 2

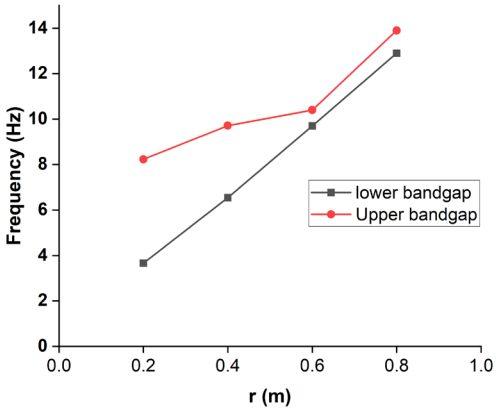

Fig. 12. Lower and upper bandgap variation with increase in circular opening "r" for model 4

4. Conclusion

The 0-20 Hz attenuation zone is very important to civil infrastructural design such as building laboratories with sensitive equipment and in its application of noise control. It is often termed low frequency vibrations, and hence critical. The investigation and modelling approach focused on seismic metamaterial with soil inclusion as this is more practical and insightful in studying the interaction within the layers. The proposed model in this study achieved bandgap with frequency belonging to the low range (0–20 Hz) at a considerable size of 2.2 meters. The mechanism of bandgap formation was associated with local resonance from the model analysis of boundaries revealing energy dissipation and deformation.

The results from previous sections have constituted the following conclusions

- Model 3 gave the best result with the widest bandgap of 2.4-6.8Hz due to the presence of the cubic hole in the lead core. The cubic opening would also reduce the lead material usage and cost implications.
- Model 4 results show the smallest width of attenuation between 12.9-13.9Hz as there was interaction between the soil layer through the circular opening that was cut through the auxetic foam.
- The geometric parameter also revealed that as the lattice constant “a” is increased with all other parameters kept constant, the band width reduces which is due to the interaction between the soil and auxetic foam

4.1. Recommendation

Several research have been done toward the behavior of SM and how it can provide solutions to existing challenges in various fields. These findings have shown the great potential that is embedded in the full adoption of SM. However, a lot more needs to be done in terms of practicability, design, regulation and scalability issues surrounding its full potential.

REFERENCES

[1] *Y. Achaoui, B. Ungureanu, S. Enoch, S. Brûlé, S. Guenneau*, Seismic waves damping with arrays of inertial resonators, Extreme Mechanics Letters, Vol. 8, No. NA, pp. 30-37, 2016, 2016.

[2] *L. Ralf,* Phononic crystals and metamaterials, Procedia Engineering, Vol. 87, pp. 40-45, 2014.

[3] *C. Qiqi, et al.*, Review of Phononic crystals and acoustic metamaterials, OP Conference Series: Materials Science and Engineering, 2020, 2020.

[4] *Zeng, et al.,* Subwavelength seismic metamaterial with an ultra-low frequency bandgap, Journal of Applied Physics, Vol. 128, No. 1, pp. 014901-NA, 2020, 2020.

[5] *I. L. Chang, Z.-X. Liang, H.-W. Kao, S.-H. Chang, C.-Y. Yang*, The wave attenuation mechanism of the periodic local resonant metamaterial, Journal of Sound and Vibration, Vol. 412, No. NA, pp. 349-359, 2018, 2018.

[6] *Brûlé, et al.*, Experiments on seismic metamaterials: molding surface waves, Physical review letters, Vol. 112, No. 13, pp. 133901-133901, 2014, 2014.

[7] *N. A. Muhammad, C. W. Lim, J. N. Reddy*, Built-up structural steel sections as seismic metamaterials for surface wave attenuation with low frequency wide bandgap in layered soil medium, Engineering Structures, Vol. 188, No. NA, pp. 440-451, 2019, 2019.

[8] *Brûlé, et al.*, Emergence of Seismic Metamaterials: Current State and Future Perspectives, Physics Letters A, Vol. 384, No. 1, pp. 126034-NA, 2020, 2020.

[9] *D. Mu, H. Shu, L. Zhao, S. An,* A Review of Research on Seismic Metamaterials, Advanced Engineering Materials, Vol. 22, No. 4, pp. 1901148-NA, 2020, 2020.

[10] *A. Ni, Z. Shi,* Broadband wave attenuation and topological transport in novel periodic pile barriers, Engineering Structures, Vol. 262, No. NA, pp. 114378-114378, 2022, 2022.

[11] *Y. I. Bobrovnitskii,* Impedance theory of wave propagation on infinite periodic structures, Journal of Sound and Vibration, Vol. 525, No. NA, pp. 116801-116801, 2022, 2022.

[12] *J. Huang, W. Liu, Z. Shi,* Surface-wave attenuation zone of layered periodic structures and feasible application in ground vibration reduction, Construction and Building Materials, Vol. 141, pp. 1-11, 2017/06//, 2017. en

[13] *Zhang, et al.*, Seismic metamaterials with cross-like and square steel sections for low-frequency wide band gaps, Engineering Structures, Vol. 232, No. NA, pp. 111870-NA, 2021, 2021.

[14] *Krödel, et al.,* Wide band-gap seismic metastructures, Extreme Mechanics Letters, Vol. 4, No. NA, pp. 111-117, 2015, 2015.

[15] *A. Colombi, P. Roux, S. Guenneau, P. Guéguen, R. V. Craster*, Forests as a natural seismic metamaterial: Rayleigh wave bandgaps induced by local resonances, Scientific reports, Vol. 6, No. 1, pp. 19238-19238, 2016, 2016.

[16] *X. Wu, Z. Wen, Y. Jin, T. Rabczuk, X. Zhuang, B. Djafari-Rouhani*, Broadband Rayleigh wave attenuation by gradient metamaterials, International Journal of Mechanical Sciences, Vol. 205, No. NA, pp. 106592-NA, 2021, 2021.

[17] *H. Jin, H. Hao, W. Chen, C. Xu*, Effect of enhanced coating layer on the bandgap characteristics and response of metaconcrete, Mechanics of Advanced Materials and Structures, Vol. 30, No. 1, pp. 175-188, 2021, 2021.

[18] *Y. Zeng, Y. Xu, K. Deng, Z. Zeng, H. Yang, M. Muzamil, Q. Du*, Low-frequency broadband seismic metamaterial using I-shaped pillars in a half-space, Journal of Applied Physics, Vol. 123, No. 21, pp. 214901-NA, 2018, 2018.

[19] *M. M. Hajjaj, J. Tu,* A seismic metamaterial concept with very short resonators using depleted uranium, Archive of Applied Mechanics, Vol. 91, No. 5, pp. 2279-2300, 2021, 2021.

[20] *E. Muzar, J. A. H. Stotz*, Surface acoustic wave modes in two-dimensional shallow void inclusion phononic crystals on GaAs, Journal of Applied Physics, Vol. 126, No. 2, pp. 025104-NA, 2019, 2019.

[21] *M. a. Lim*, Phononic metastructures with ultrawide low frequency three-dimensional bandgaps as broadband low frequency filter, Sci. Rep., 2021, Vol. Wave propagation in periodic structures: Electric filters, 2021.

[22] *X. Pu, Z. Shi, H. Xiang*, Feasibility of ambient vibration screening by periodic geofoam-filled trenches, Soil Dynamics and Earthquake Engineering, Vol. 104, No. NA, pp. 228-235, 2018, 2018.

[23] *J. Castro, C. Sagaseta,* Consolidation around stone columns. Influence of column deformation, International Journal for Numerical and Analytical Methods in Geomechanics, Vol. 33, No. 7, pp. 851-877, 2008, 2008.

[24] N. Sharafkhani, A Helmholtz Resonator-Based Acoustic Metamaterial for Power Transformer Noise Control, *Acoustics Australia,* Vol. 50, No. 1, pp. 71-77, 2021, 2021.

[25] *S. Kaçın, M. Öztürk, U. K. Sevim, M. Karaaslan, Z. Özer, O. Akgöl, B. A. Mert, E. Üna*l, Experimental verification of phononic crystal based on square arrays of cylindrical holes against seismic vibrations in full-scale systems: modeling, sensing and signal processing of seismic vibrations, Archive of Applied Mechanics, Vol. 92, No. 1, pp. 309-323, 2021, 2021.

[26] *B. B. Alagoz, S. Alagoz,* Towards Earthquake Shields: A Numerical Investigation of Earthquake Shielding with Seismic Crystals, Open Journal of Acoustics*,* Vol. 01, No. 3, pp. 63-69, 2011, 2011.

[27] *A. Thakur, A. Gupta*, Computational study of seismic wave propagation through metamaterial foundation, International Journal for Computational Methods in Engineering Science and Mechanics, Vol. 22, No. 3, pp. 200-207, 2021, 2021.

[28] *M. Nouh, O. J. Aldraihem, A. M. Baz,* Vibration Characteristics of Metamaterial Beams With Periodic Local Resonances, Journal of Vibration and Acoustics*,* Vol. 136, No. 6, pp. 061012-NA, 2014, 2014.

[29] *B. M. V. L. X. C. Y. H. G. Xu X,* Tailoring vibration suppression bands with hierarchical metamaterials containing local resonators, 2019, 2019.

[30] *B. Ungureanu, Y. Achaoui, S. Enoch, S. Brûlé, S. Guenneau*, Auxetic-like metamaterials as novel earthquake protections, EPJ Applied Metamaterials*,* Vol. 2, No. NA, pp. 17-NA, 2015, 2015.

[31] *Hsu, et al.,* Local resonances-induced low-frequency band gaps in two-dimensional phononic crystal slabs with periodic stepped resonators, Journal of Physics D: Applied Physics, Vol. 44, No. 5, pp. 055401-NA, 2011, 2011.

[32] *T. V. Varma, B. Ungureanu, S. Sarkar, R. V. Craster, S. Guenneau, S. Brûlé*, The Influence of Clamping, Structure Geometry, and Material on Seismic Metamaterial Performance, Frontiers in Materials*,* Vol. 8, No. NA, pp. 603820-NA, 2021, 2021.

[33] *N. A. Muhammad, C. W. Lim, K. K. Żur,* Wide Rayleigh waves bandgap engineered metabarriers for ground born vibration attenuation, Engineering Structures, Vol. 246, No. NA, pp. 113019-NA, 2021, 2021.

[34] *Q. Du, Y. Zeng, G. Huang, H. Yang*, Elastic metamaterial-based seismic shield for both Lamb and surface waves, AIP Advances*,* Vol. 7, No. 7, pp. 075015-NA, 2017, 2017.

[35] *L. Brillouin,* 1953, Wave propagation in periodic structures: Electric filters and crystal lattices. ,

[36] *N. Shi, H. Liu, L. Zhao*, Novel small-size seismic metamaterial with ultra-low frequency bandgap for Lamb waves, Europhysics Letters, Vol. 147, No. 4, pp. 42002, 2024/08/27/, 2024.

[37] *Akintoye, et al.*, Vibro stone as periodic wave barriers for train-induced vibration attenuation of Lamb and surface waves, 2024.